Article

aeroacoustics

Aerodynamic noise from an asymmetric airfoil with perforated extension plates at the trailing edge

International Journal of Aeroacoustics
0(0) 1–21

DOI: 10.1177/1475472X20978388
journals.sagepub.com/home/jae
SAGE

CK Sumesh and TJS Jothi

Abstract

This paper investigates the noise emissions from NACA 6412 asymmetric airfoil with different perforated extension plates at the trailing edge. The length of the extension plate is 10 mm, and the pore diameters (D) considered for the study are in the range of 0.689 to 1.665 mm. The experiments are carried out in the flow velocity (U_∞) range of 20 to 45 m/s, and geometric angles of attack (α_g) values of -10° to $+10^\circ$. Perforated extensions have an overwhelming response in reducing the low frequency noise ($<$1.5 kHz), and a reduction of up to 6 dB is observed with an increase in the pore diameter. Contrastingly, the higher frequency noise ($>$4 kHz) is observed to increase with an increase in the pore diameter. The dominant reduction in the low frequency noise for perforated model airfoils is within the Strouhal number (based on the displacement thickness) of 0.11. The overall sound pressure levels of perforated model airfoils are observed to reduce by a maximum of 2 dB compared to the base airfoil. Finally, by varying the geometric angle of attack from -10° to $+10^\circ$, the lower frequency noise is seen to increase, while the high frequency noise is observed to decrease.

Keywords

Asymmetric airfoil, perforations, trailing edge noise, pore diameter, open area ratio

Date received: 28 August 2020; accepted: 8 November 2020

Department of Mechanical Engineering, National Institute of Technology Calicut, Kozhikode, India

Corresponding author:
TJS Jothi, Department of Mechanical Engineering, National Institute of Technology Calicut, Kozhikode, Kerala 673601, India.
Email: tjsjothi@nitc.ac.in

Introduction

Aerodynamic noise generated from airplane wings is an important noise source, and there is a considerable demand for a viable noise reduction mechanism. Numerous research works are carried out to address the noise emission from airfoils. One of the major noise sources is the trailing edge interaction noise, where the flow structures in the turbulent boundary layer over an airfoil interacts with the sharp trailing edge, thus generating the noise.[1] The trailing edge interaction noise has been studied by numerous researchers in subsequent years.[2–5] Several active and passive techniques are introduced to reduce the trailing edge noise by modifying the flow field and the scattering efficiency. Active methods include blowing/suction of fluid at the trailing edge, external acoustic excitation, and plasma actuators.[6–8] Various passive techniques, such as serrations, porosity, and brushes at the trailing edge,[9–11] having different surface impedances, are used for trailing edge noise reduction. The reason for the noise reduction is stated as the minimal scattering at the trailing edge. Hayden[12] observed that a solid surface has a larger impedance, and its sudden discontinuity at the trailing edge enhances the scattering of the flow structures. This scattering efficiency is seen to reduce by varying the surface impedance using the porous treatments and thus mitigating the trailing edge noise. Bohn[13] carried out experimental investigations in the noise generated from a flat plate equipped with porous extensions in the streamwise direction of varying lengths at the trailing edge. He found that the noise reduction is frequency dependent and is inversely proportional to the length of the flow wise extension, and the noise reduction is due to the edge impedance control by an acoustic feedback mechanism. Owls are well known for their silent flight, and the reason is attributed to the porosity nature of its feathers that help in moving the flow from the pressure side to the suction side of the wing.[14] An Experimental study by Chanaud et al.[15] reveals that the fan noise can be reduced by 5 dB using porous blades compared to that of a solid blade. Fink and Bailey[16] carried out experiments on a wing model with perforated slat and flap and found a substantial reduction in the airframe noise. Khorrami et al.[17] numerically studied the effectiveness of the porous rotor tip treatment for the reduction of tip clearance noise in a turbofan engine. Interestingly, the modification considerably reduced the noise just by altering the tip clearance. Further, they reported a noise reduction of more than 20 dB without much penalty on the aerodynamic performance.[18] The effect of different porous airfoil on the trailing edge noise reduction was experimentally analysed by Sarradj and Geyer[10] and reported a noise reduction up to 10 dB. They found that the noise reduction potential strongly depends on the porous material properties like porosity and resistivity. Herr and co-workers[19,20] conducted acoustic experiments on flow-permeable trailing edges and showed the noise reduction potential of permeable materials at the trailing edge of the airfoil. Geyer et al.[21] studied the influence of porous material's flow resistivity and established a relation between the boundary layer parameters and noise reduction by the porous airfoil. The fully permeable airfoil performs well on noise reduction but loses its aerodynamic performance compared to a baseline airfoil. To overcome this limitation, Geyer and Sarradj[22] used porous material only to the trailing edge to make the airfoil partially porous and observed a far-field noise reduction up to 8 dB with a negligible lift loss. The noise reduction capacity of the porous material on vortex shedding tones and edge scattering noise by the convected eddies has been numerically studied by Bae and Moon[23] and reported a 3 dB reduction in vortex shedding tonal peaks by breaking the special correlation of wall pressure fluctuations alongside the trailing edge. Similarly, the porous material weakens the pressure fluctuations at the

trailing edge that leads to 3 ~10 dB reduction in edge scattering noise in a wide frequency range. Jaworski and Peake[24] conducted analytical studies to point out the effect of porosity and elasticity on the interaction of turbulent structures with a semi-infinite poroelastic edge and scaling behaviour of the trailing edge noise with flow properties using Wiener–Hopf technique. Their results revealed that the far-field acoustic power has a scaling dependency of U^6 with the porous edge and U^7 with the elastic edge, compared to the U^5 dependence of a rigid impermeable edge. Further, Herr et al.[25] conducted acoustic tests on a DLRF 16 airfoil model with a large variety of porous inserts at the trailing edge region 10% of the chord. They reported a maximum broadband noise reduction of 2–6 dB with respect to the baseline at frequencies less than 10 kHz and has a strong dependence on flow resistivity. An increase in noise above 10 kHz is due to the surface roughness offered by the porous inserts. To control the trailing edge scattering noise, Kisil and Ayton[26] reported that the finite flat porous extensions on an impermeable trailing edge mitigate the noise due to the interaction of a convective gust at the trailing edge in a uniform steady flow. Jiang et al.[27] carried out wind tunnel experiments on blades with integrated porosity at the trailing edge to find out the effectiveness on the acoustic scattering. They found that the pore geometry and aspect ratio have a substantial impact on noise reduction.

The experimental studies conducted by Ali et al.[28] on a flat plate with a porous trailing edge insert revealed a significant reduction in the energy of the low frequency structures within the boundary layer. The presence of a permeable surface significantly reduces the spanwise coherence of these structures and leads to the abatement of scattering noise as well as the vortex shedding noise from a blunt trailing edge. The hydrodynamic and acoustic fields of a solid and porous metal foam trailing edge insert of a NACA 0018 airfoil were experimentally investigated by Carpio et al.[29] Their findings reveal that a larger permeability imparts higher attenuation in a shorter frequency range ($f < 1.6$ kHz), while a smaller permeability provides lower attenuation for a wider frequency range ($f < 1.9$ kHz), and an increase in noise beyond these frequencies. The results also revealed that for lower permeability inserts, the turbulent intensity and eddy convection velocity is observed to reduce compared to the solid trailing edge, which decreases the low frequency noise. The effect of wall normal permeable trailing edge on the turbulent boundary layer noise generation is investigated by Zhang and Chong.[30] They suggested that since the noise sources are located very close to the trailing edge, a small porous coverage is sufficient to obtain an appreciable noise reduction, and reported a maximum noise reduction of 7 dB. Sumesh and Jothi[31] discussed the noise characteristics of a thin airfoil having a line distribution of holes adjacent to the trailing edge. The considered airfoil is found to be effective in decreasing the low frequency noise up to the Strouhal number (based on the boundary layer thickness) of 0.15. Recently, Zhang and Chong[32] investigated the laminar instability noise emissions in NACA 65(12)–10 airfoil having a porous trailing edge with the pore diameters of 1, 2, and 3 mm. They found that the broadband noise levels depend upon the hole diameters and the length of the porous trailing edge. At a lower Reynolds number, the noise is seen to decrease with the decrease in the hole diameter and increase with porous trailing edge length.

Porous treatments in airfoils are found to be beneficial in reducing the trailing edge noise from airfoils. Numerous literature have discussed the mitigation of airfoil noise using the porous structures, and the summary of the different porous conditions used by the researchers in the past are tabulated in Table 1. In line with the works carried out in the literature on the modifications of a trailing edge using a porous medium, the present work illustrates the effect of perforations in the extension plates at the trailing edge over noise reductions. Albeit the porous medium is widely utilised in the noise reductions in airfoils, the effect of perforated

Table 1. Features of the different porous mediums used by the researchers for noise reductions in airfoils.

Sl no.	Literature	Modifications in airfoil	Pore diameter (mm)
1	Chanaud et al.[15]	Porous material fan blades	0.165 and 0.065
2	Fink and Baily[16]	Perforated trailing edge	0.061
3	Herr and Reichenberger[20]	Perforated plate at trailing edge	0.11
4	Herr et al.[25]	Porous material at trailing edge	0.1, 0.16, and 0.026
5	Jiang et al.[27]	Perforated trailing edge	0.8
6	Carpio et al.[29]	Porous material at trailing edge	0.45 and 0.8
7	Sumesh and Jothi[31]	Line distribution of circular holes adjacent to the trailing edge	3
8	Zhang and Chong[32]	3D circular pore pattern at trailing edge	1, 2, and 3
9	Suryadi et al.[33]	Micro-perforated plate extensions at the trailing edge	0.1 and 0.162
10	Carpio et al.[34]	3D circular pore pattern at trailing edge	0.8

trailing edge plate on noise emissions is rarely investigated. The authors carried out a similar study on noise reductions from a thin airfoil using a line distribution of holes adjacent to the trailing edge.[31] However, the hole size considered was higher (3 mm diameter) and distributed in a single line, while in the present study, perforated extension plates with a gradual variation of the surface impedance are considered. A thin plate is extended from the trailing edge of an airfoil for a length of 10 mm. The extension plates have uniform diameter pores and are in the range of 0.689 to 1.665 mm. This paper investigates the systematic variation of the pore diameters on the low- and high-frequency noise emissions from a NACA 6412 asymmetric airfoil. Four plates of different pore diameters are considered for the noise study, and their comparisons are made with the airfoil with a solid plate (no perforations) and a base model airfoil (without an extension plate).

Experimental setup and instrumentation

Anechoic test facility

Far-field noise measurements are carried out in a semi-anechoic chamber facility of dimensions $2.6\,\text{m} \times 2.6\,\text{m} \times 2.6\,\text{m}$, as shown in Figure 1(a). The anechoic chamber walls are adhered with a wedge made of polyurethane foam. The anechoic chamber is found to have a cut-off frequency of 300 Hz. An open-wind tunnel facility is erected inside the chamber, where the airfoil test models are mounted for experimentation. Air is supplied to the test-section by a cubically contoured nozzle having exit dimensions of 80 mm in height and 200 mm in width. The flow velocity (U_∞) is varied from 20 to 45 m/s, and the corresponding Reynolds number (Re_c) based on the chord is in the range of 1.9×10^5 to 4.2×10^5. The turbulent intensity measured at the centre of the nozzle exit plane is estimated to be around 0.2%. The airfoil is mounted in the test-section with its leading edge positioned at a downstream distance of 25 mm from the nozzle exit, as shown in Figure 1(b), to minimize the turbulent flow interactions at the leading edge. Further, the airfoil is placed between two side plates in the test section to maintain a two-dimensional flow around the airfoil (Figure 2). To avoid an additional noise due to the side plates, the airfoil has a span length larger than the width of the nozzle exit. The considered height of the nozzle ensures that the free shear layer

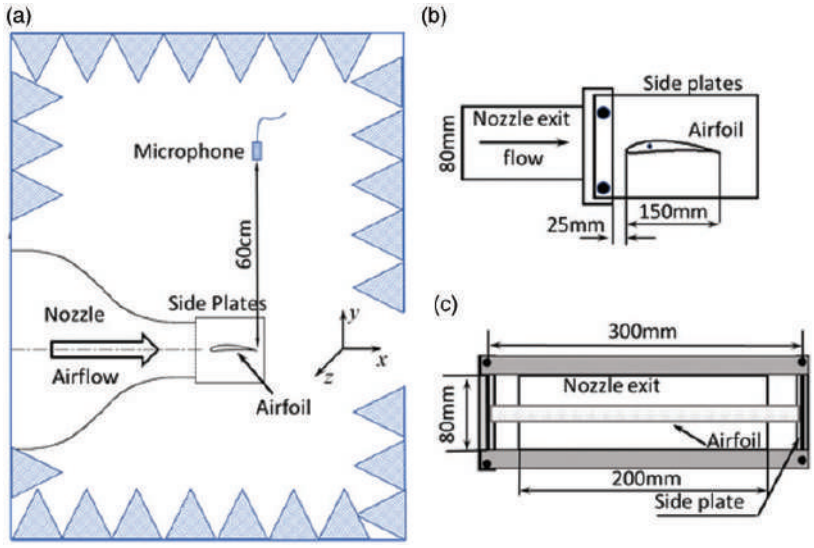

Figure 1. (a) Schematic diagram of the experimental setup, (b) side view of the test section, (c) front view of the test section.

generated from the nozzle lips does not interact with the trailing edge, thus ensuring that the entire airfoil is within the potential core of the free jet.

Test models

A NACA 6412 airfoil model is used for the experiments in the present study, which is fabricated using the wire cut electro-discharge machining process. The airfoil is made of aluminium material, having a chord (c) of 150 mm and a span of 300 mm (Figure 3(a)). The trailing edge of the airfoil has a thin slit of $\sim$0.5 mm along its span to accommodate the extension plates. In the present study, four extension plates having different pore diameters are considered and are designated as M1, M2, M3, and M4 models (Figure 3(b)). The M1 model has the least pore diameter of 0.689 mm, and the M4 model with the largest pore diameter is 1.665 mm. In addition, a solid extension plate with no perforation is considered and is designated as M0. All the plates are 0.4 mm thick and are inserted into the airfoil slit as a tight-fit with 10 mm projecting out of the trailing edge (Figure 3(a)). The noise from the above extension plate airfoils is compared with a base model airfoil with no extension plate attached. The different plates used in the study and their perforation features are shown in Table 2, which are measured from a 2 D microscopic surface images (Figure 4) taken using a 3 D optical profilometer (Alicona make). All the models have the pores staggered in an equilateral triangular array pattern, as shown in Figure 4. A fractional open area, β, of a perforated plate is defined as the ratio of an open area to the total area of the plate. In general, for a plate with a uniform distribution of constant diameter pores with a triangular pattern arrangement, the open area ratio is expressed as,

$$\beta\ (\%) = \frac{\pi \times D^2}{2\sqrt{3}P^2} \tag{1}$$

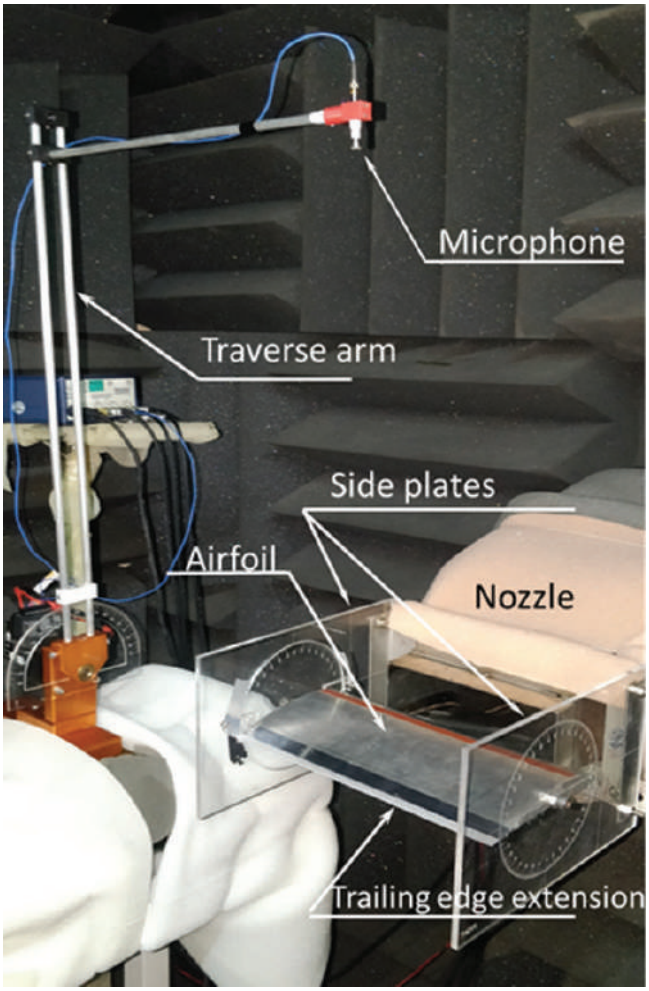

Figure 2. Photograph of an experimental setup.

where P is a pitch (spacing between the centres of the closest holes).[35] The pore diameter is seen to gradually increase for M1 to M4 airfoil models, as noted in Table 2; however, their open area ratio variation is not uniform. Since the pitch of all the perforated models is different, the open area ratio increases up to the M3 model, and the M4 model has the least open area ratio. This variation calls for a discussion on the effect of an open area ratio on the noise emissions. Therefore, as a special case, an additional perforated model (M2*) with almost the same pore diameter as of M2 ($\sim$0.876) but with a lower open area ratio is considered to study the effect of open area ratio on the noise emissions. Their respective open area ratios are 42.9% and 45.6% (Table 2). The boundary layer formed over the airfoil is tripped by a roughness tape adhered along the span to ensure a fully turbulent boundary layer over the airfoil (Figure 2), and circumvent tonal noise due to the laminar boundary layer and its instability. Therefore, the only aerodynamic noise source is speculated as to the trailing edge scattering noise. The tape is 10 mm in width and 0.4 mm in thickness and has a

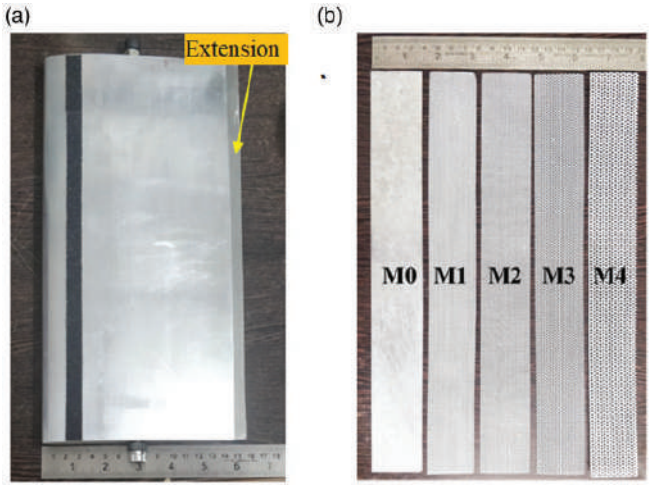

Figure 3. (a) Airfoil model with an extension plate inserted, and (b) different extension plates considered for the study.

Table 2. Properties of the perforated plates used for experiments.

Sl.No.	Designation of perforated plates	Pore Diameter (D) (mm)	Pitch of perforations (P) (mm)	Open area ratio (β) (%)	Holes per square inch
1	M0	0	0	0	0
2	M1	0.689	0.991	43.8	759
3	M2	0.876	1.235	45.6	489
4	M3	1.290	1.793	46.9	232
5	M4	1.665	2.544	38.8	115
6	M2*	0.874	1.270	42.9	462

roughness of 140 μm. The boundary layer trip is located at 20% of the chord from the leading edge on both the pressure and suction sides of the airfoil. In order to ensure a smooth flow over the extended plates, the small interfacing step is covered by a thin aluminium adhesive tape on both sides of the airfoil.

Instrumentation and measurement procedure

The acoustic measurements are carried out using a quarter-inch condenser microphone of PCB make (model No 378C01) at a polar angle of 90°. The microphone is positioned at $y/c \approx 4$ above the midspan of the trailing edge for all the airfoil experiments, as seen in Figure 1. The geometric angle of attack is varied from -10° to 10° at 5° intervals. The microphone is connected to a 16-bit NI-DAQ card (NI PCI-6143), and the data are acquired at a sampling rate of 150 kHz for a time duration of 10 seconds. The data is acquired using the LabView software, and the post-processing is carried out using the Matlab software. Acoustic spectra are plotted by carrying out the Fast Fourier Transform of the data with a bin-width of 4096

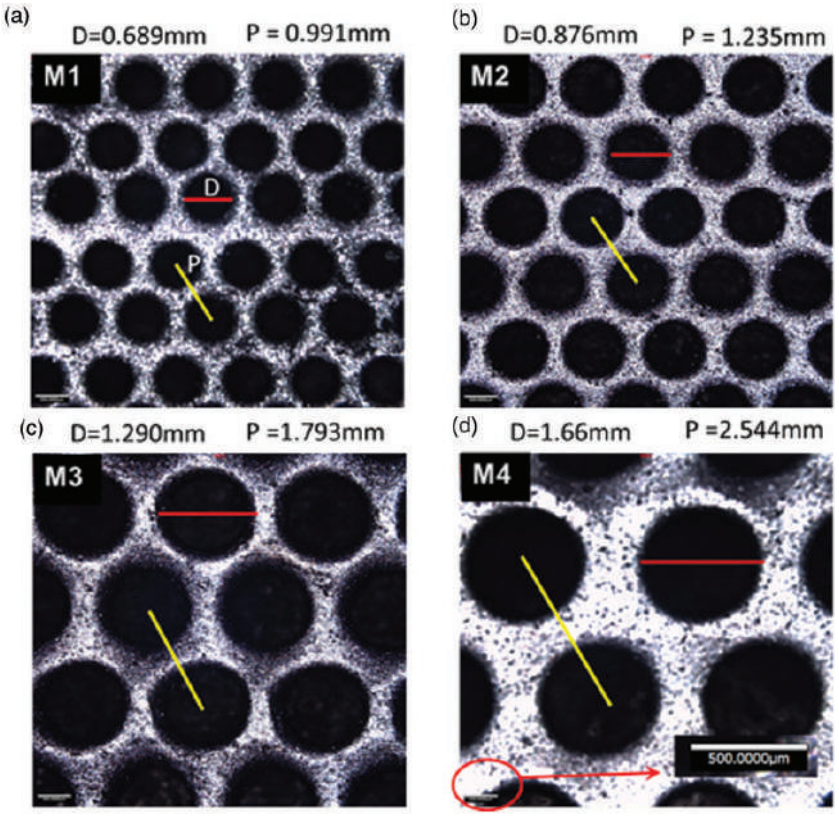

Figure 4. Microscopic images of the perforated plates, namely, (a) M1, (b) M2, (c) M3, and (d) M4.

samples resulting in a frequency resolution of 36.62 Hz. The acoustic spectra are expressed as the power spectral density (PSD) in dB/Hz by normalising the far-field acoustic pressure with a reference pressure of 20 µPa. All the spectra in the present study are plotted with a minimum frequency of 300 Hz as it corresponds to the cut-off frequency of the anechoic chamber. Repeated experiments at different times resulted in an uncertainty of ±0.5 dB in estimating the OASPL.

Results and discussion

This section describes the acoustic results of an airfoil attached with the different extension plates and compared with the base model airfoil at different flow velocities and angles of attack. Since the free stream turbulence of the flow approaching the leading edge is less than 0.2%, and the side walls are not in the vicinity of the jet flow, the leading-edge noise may not be the dominant noise source.[36]

Noise from base model airfoil

This section investigates the noise emission from the NACA 6412 - base model airfoil. Figure 5(a) compares the acoustic spectra of the base model airfoil and the background

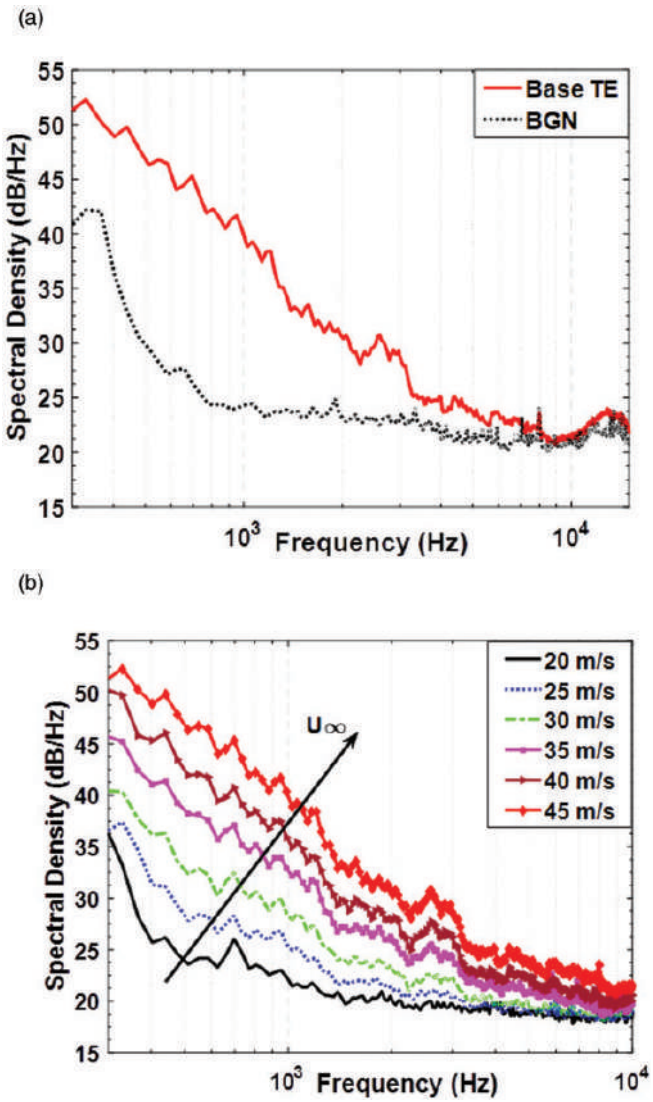

Figure 5. (a) Spectral comparison of airfoil noise with the background noise at $U_\infty = 45$ m/s. (b) Spectra of the base model airfoil at different flow velocities.

noise (without airfoil) at the flow velocity of 45 m/s. The noise levels of the base model airfoil are well above the background noise (BGN) in the frequency range of 0.3 to 6 kHz. Therefore, the acoustic spectra of airfoil noise are least contaminated by the background noise in this frequency range, and the primary noise source is the trailing edge scattering noise. The two spectra are observed to collapse above 6 kHz, and the noise above this frequency can be safely neglected. Therefore, all the one third band spectra are plotted by subtracting the background noise. Figure 5(b) shows the spectra of the base model airfoil at zero angle of attack and different flow velocities. The noise levels gradually increase with an

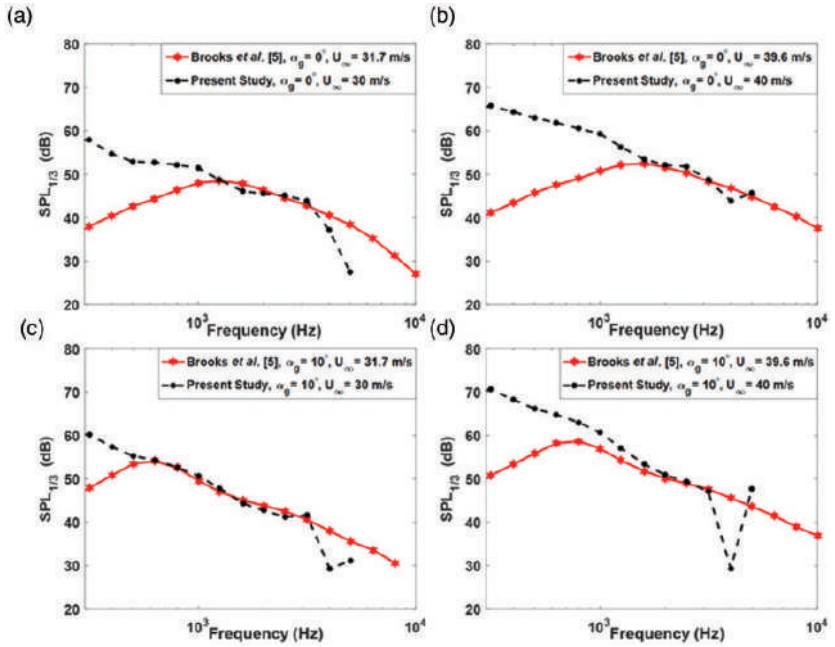

Figure 6. Comparison of the acoustic spectra of the base model airfoil with those of the predicted trailing edge scattering noise of NACA0012 airfoil[5] at different conditions.

increase in the flow velocity, more pertinently at frequencies below 3 kHz. In addition, a broadband hump is observed with a centre frequency of ~2.6 kHz at the flow velocities greater than 30 m/s. Since the centre frequency does not vary with the flow velocity, it is conjectured that this noise is induced by the experimental facility. Since the trailing edge is blunt with a thickness of ~0.5 mm, the vortex shedding noise is avoided, as no tones are noted in the spectra. The self-noise mechanism of the base model airfoil is compared with the trailing edge scattering noise prediction of NACA 0012 airfoil by Brooks et al.[5] in Figure 6 for flow velocities of 30 and 40 m/s, and angles of attack of 0 and 10 degrees. The trailing edge noise is observed to match with the predictions of Brooks et al.[5] in the range of 1–3 kHz at all velocities and angles of attack, however, with slight variations, which could probably be due to the different airfoil shapes and measurement locations.

Figure 7 provides the scaled spectral plots of the base model airfoil at different flow velocities. The scaling analysis is carried out based on the simplest noise reduction strategy by Ffowcs-Williams and Hall,[2] where they showed that the trailing edge noise is observed to scale with the fifth power of free-stream velocity (U_∞). Further, it is also noticed that the flow structures of the order of boundary layer thickness induce the trailing edge scattering noise.[37] For the present base model airfoil, the one-third octave band Sound Pressure Levels (SPL) spectra are calculated at different flow velocities and is scaled with the fifth power of the flow velocity and boundary layer displacement thickness δ^*, given as,

$$SPL_{1/3\ Scaled} = SPL_{1/3} - 50\log_{10}\left(\frac{U}{U_\infty}\right) - 10\log_{10}\left(\frac{\delta^*}{\delta_{ref}}\right) \quad (2)$$

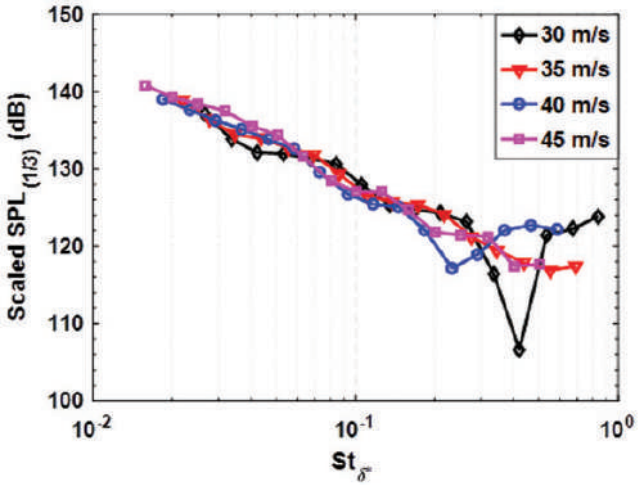

Figure 7. Normalised one-third octave band noise spectra of base model airfoil.

and

$$St_{\delta^*} = \frac{f_c\ \delta^*}{U_\infty} \tag{3}$$

where $St_{\delta*}$ is the Strouhal Number based on the boundary layer displacement thickness δ* and δ_{ref} is the unit reference length for the SPL normalization.[19] The displacement thickness over the airfoil models at different flow velocities is estimated using the XFOIL.[38] The spectra are seen to collapse well in the Strouhal number range of $\sim$0.01 and 0.15, which signifies that the trailing edge noise is majorly contributed by the flow velocity and the boundary layer parameter.

Noise from airfoils with extensions

This section describes the noise from different model airfoils and their comparison with the base model airfoil. Figure 8 compares the spectra of different model airfoils with the base model airfoil at 45 m/s. Interestingly, the M0 model airfoil has the highest noise levels compared to the base model and other perforated model airfoils at frequencies below $\sim$ 1.5 kHz. This is because the M0 model airfoil is without perforations, and it effectively increases the chord length of the airfoil. This increases the lower frequency noise levels due to an enhancement in the large eddy fluctuations at the trailing edge.[39] The gradient of the M0 model airfoil is observed to be similar to that of the base model airfoil, which indicates that the noise generation mechanism is not altered due to the modification. Further, the M0 model airfoil results in an acoustic scattering at the trailing edge due to the sudden impedance mismatch similar to that of the base airfoil.[40] An increase in the pore diameter leads to a gradual decrease in the low frequency noise below $\sim$ 1.5 kHz (Figure 8) due to a decrease in the surface impedance of the airfoil models from M1 to M4. This indicates that the perforations reduce the turbulent fluctuations, thus reducing the low

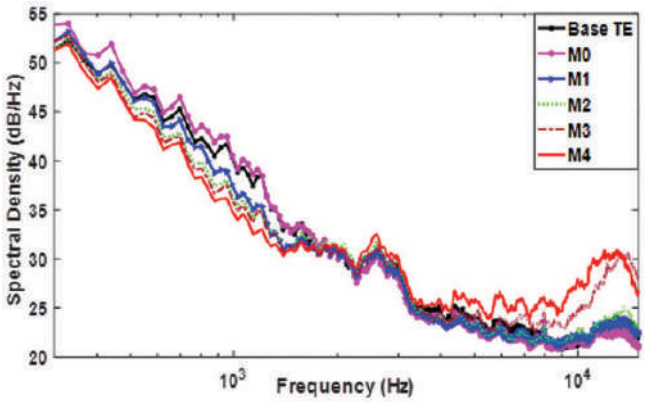

Figure 8. Narrowband spectral comparison of different perforated model airfoils at $U_\infty = 45$ m/s.

frequency noise.[26] Further, the reduction in the low frequency noise is also corroborated to the decrease in the scattering efficiency at the trailing edge, as the slopes of the spectra of perforated model airfoils show a gradual variation with an increase in the pore size.[26,29] The spectra in the frequency range of 1.5 to 2.2 kHz are almost the same for all the airfoil models, which is speculated to the scattering of small-scale eddies over the airfoil, and this noise is unaffected to the presence of the perforations.[23] The comparison of the high frequency noise above 4 kHz indicates that noise levels of M0, M1, and M2 model airfoils are almost similar, while M3 and M4 model airfoils have higher noise levels. The reason for this noise is speculated to the roughness effect offered by the cross-flow through the higher diameter pores (M3 and M4 models) compared to the lower diameter pore models.[21,22,29]

To quantify the noise attenuated by the different perforated model airfoils (M1 to M4), the reduction in their noise levels (ΔSPL), which is the difference in the sound pressure levels of the base model and perforated model airfoils are plotted as a contour plot in Figure 9 as a function of the free stream velocity. The positive ΔSPL in the contour map represents the effectiveness of the perforated extension model airfoils in reducing the trailing edge scattering noise. All spectra show a dominant noise in the frequency range of 0.3 to 2 kHz. A dashed line in Figure 9 represents a demarcation of a high and low ΔSPL region in the spectra and connects the loci where the Strouhal number $St_{\delta*}$ is 0.11. The region $St_{\delta*} < 0.11$ represents the trailing edge noise, which is in congruence with the literature.[41] The spectral contours reveal that all the perforated airfoil models have noise levels below the base model in the lower frequency region. With an increase in the pore size, the noise levels from the perforated model airfoil decrease. The maximum noise reduction for the M1 model airfoil is around 4 – 5 dB and is seen to gradually increase with an increase in the pore diameter. A maximum reduction is observed to be around 6 dB for the M4 model airfoil. Further, the dominancy in the higher frequency noise by the perforated model airfoils is noted at the higher velocities for M3 and M4 model airfoils, however feeble for M1 and M2 cases. The high frequency noise of M3 and M4 models is larger by around 7 – 8 dB compared to the base model airfoil at flow velocities higher than 35 m/s. The reduction in the low-frequency noise is observed at most of the flow velocities, while the high-frequency noise is noted only at velocities above 30 m/s. Thus, all the perforated model airfoils help to reduce the trailing edge noise, however, with a compromise in the emission of the higher frequency noise for

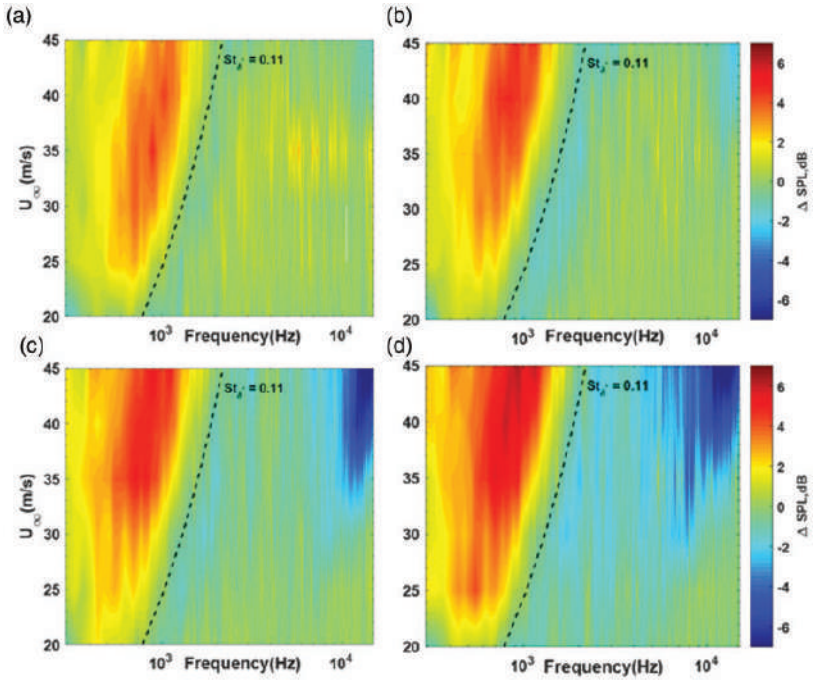

Figure 9. ΔSPL spectral contours of (a) M1, (b) M2, (c) M3, and (d) M4 model airfoils.

larger pore diameters airfoils at higher velocities.[21] As stated earlier in Table 2, the M4 model airfoil has the least open area ratio than the other perforated model airfoils. Therefore, to investigate the open area ratio dependence on noise, the spectral comparisons are made for (i) M2 and M2* model airfoils having a similar pore diameter and different open area ratios (45.6% and 42.9%, respectively), and (ii) M1 and M2* model airfoils having an approximately a similar open area ratio and different pore diameters (0.689 and 0.874 mm, respectively). These spectral comparisons are plotted in Figure 10 at the flow velocities of 40 and 45 m/s. The spectra of M2 and M2* model airfoils are almost identical, with no appreciable difference at both velocities. The comparison of M1 and M2* model airfoils indicate that the low frequency noise of the former airfoil is higher than the latter. These comparisons conclude the fact that the noise reduction largely depends on pore diameter rather than the open area ratio, which is in congruence with the findings of Herr et al.[25]

The ΔSPL spectra of the perforated model airfoils (M1 to M4) at a flow velocity of 45 m/s are shown in Figure 11(a). The positive ΔSPL indicates the effectiveness of the higher diameter pores in reducing the noise emissions within the frequency of 1.5 kHz. Further, the ΔSPL gradually increases with frequency, and a maximum reduction of 6 dB is observed at around 1.2 kHz for the M4 model airfoil. The ΔSPL in the frequency range of 1.5 to 2.2 kHz is almost similar for all perforated model airfoils, speculated to the scattering of small-scale eddies over the airfoil.[23] Beyond 3 kHz, ΔSPL is negative, thus indicating the fact that the perforations are insignificant in reducing higher frequency noise. Moreover, the high frequency noise tends to increase with an increase in the pore diameter, as discussed

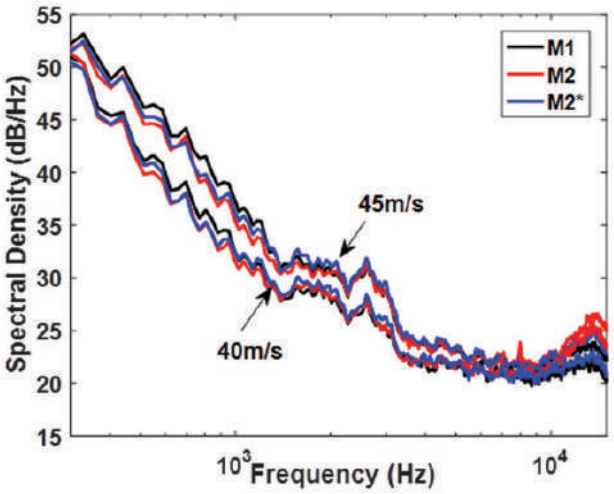

Figure 10. Spectral comparison of M1, M2 and M2* model airfoils at different velocities.

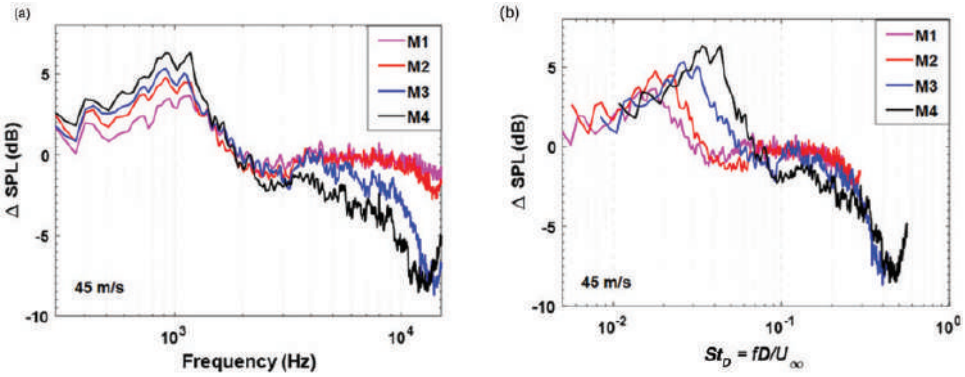

Figure 11. (a) ΔSPL spectra, and (b) scaled spectra of different perforated model airfoils at $U_\infty = 45$ m/s.

in Figure 8. The M4 model airfoil having the largest pore diameter is observed to have higher frequency noise by around 6 dB. This leads to an important conclusion that a larger pore diameter model airfoil (M4) suppresses the lower frequency noise and increases the high frequency noise. In the case of a smaller pore diameter airfoil (M1), the increase in the higher frequency noise is negligible, and the lower frequency noise reduction is considerable. Figure 11(b) shows the ΔSPL plotted against the Strouhal number (St_D) based on the pore diameter D and flow velocity U_∞. These ΔSPL spectra show a good collapse in lower and higher Strouhal number range of $St_D < 0.03$, and $0.1 \leq St_D \leq 0.4$, respectively. This depicts the fact that both the lower and higher frequency noise is influenced by the pore diameter of the perforated models, as discussed in the earlier sections.

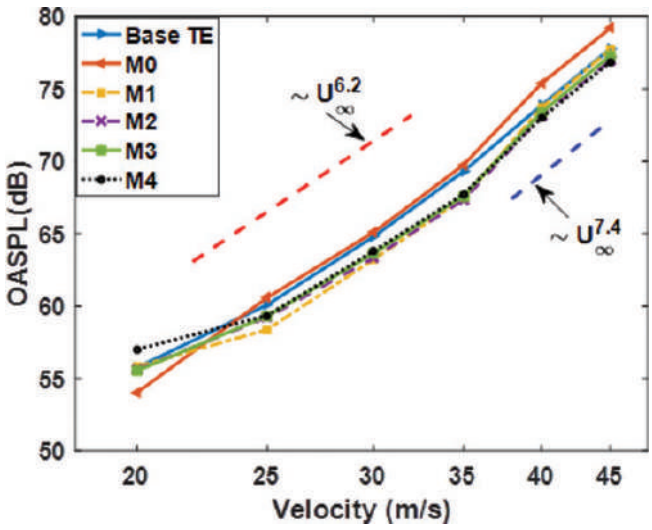

Figure 12. Variation of OASPL with flow velocity for different perforated model airfoils.

Sound pressure level studies

The Overall Sound Pressure Level (OASPL) is calculated by integrating the mean square acoustic pressure over the frequency range of 0.3 to 15 kHz and is plotted in Figure 12 for different airfoil models with free stream velocity. The M0 model airfoil shows higher OASPL above 25 m/s when compared to perforated model airfoils and the base airfoil. Interestingly, the OASPL of all the model airfoils are observed to have similar variation for $U_\infty \geq 25$ m/s. In the velocity range of 25 to 35 m/s, the OASPL of all the model airfoils has a velocity dependence of $\sim U_\infty^{6.2}$, and beyond 35 m/s, the velocity dependence shifts to $\sim U_\infty^{7.4}$. Since the OASPL variation in the former is proportional to the sixth power of the velocity approximately, the corresponding noise could be due to turbulence scattering, which behaves like a dipole source is in congruence with the findings of Jaworski and Peake.[24] The OASPL dependence on $\sim U_\infty^{7.4}$ at higher velocities is presumed to the combined effect of weaker quadrupole noise sources due to an increase in the effective chord length of the airfoil, and shear layer noise from the nozzle lip.[42] Further, all perforated model airfoils show a reduction in OASPL as compared to the base airfoil.

It is understood that the perforated model airfoils efficiently reduce the lower frequency noise, however increasing the higher frequency noise. Therefore, it is important to characterize the performance of these airfoils in their respective frequency regions, where the corresponding noise is dominant. The sound pressure levels are evaluated in the two frequency bands, namely, (i) a low frequency band in the range of $0.3 < f_L < 2.2$ kHz, and (ii) a high frequency band in the range of $8 < f_H < 15$ kHz. The ratio of the sound pressure levels of the extension model and the base model airfoils in the low frequency band (f_L) is shown in Figure 13(a). At most of the velocities, the low frequency noise from the M0 model airfoil is higher than the base model airfoil. The perforated model airfoils show a lower noise at all the velocities above 25 m/s compared to the base model airfoil, as their ratios are observed to be lower than unity. The low frequency noise attenuation is prominent in the velocity range of 25 – 35 m/s, which may be due to the cross-flow across the perforations, which effectively

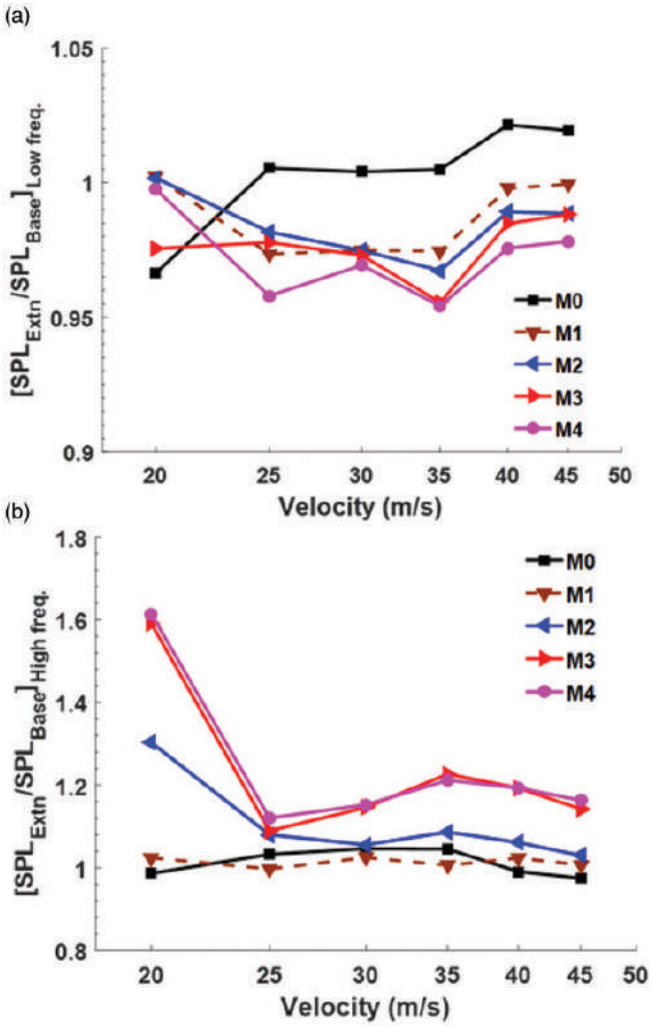

Figure 13. Variation of the ratios of (a) low frequency SPL and (b) high frequency SPL.

reduces the scattering efficiency. Beyond 35 m/s, the surface impedance of the perforated models is expected to increase with velocity,[43] thus lowering the noise attenuation. Similarly, Figure 13(b) plots the ratio of sound pressure levels in the high frequency band (f_H) for the extension model airfoils to the base model airfoil. Apparently, no extension model airfoils have a high frequency noise lower than the base model airfoil. The high frequency noise levels of M0 - M2 model airfoils are comparable to the base model airfoil at different velocities, while the same for M3 and M4 models are much larger (Figure 13(b)). The increased surface roughness due to the higher pore diameter attributes to the high frequency noise.[21,22,29] These discussions concluded that the perforations help in reducing the low frequency noise and increase the high frequency noise.

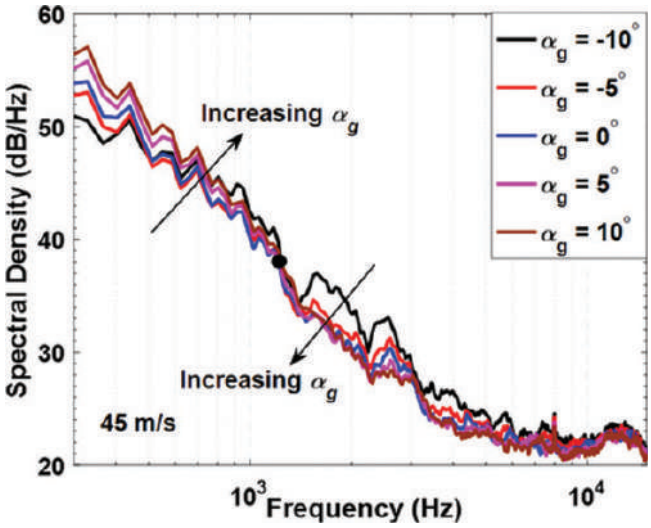

Figure 14. Spectra of the base model airfoil at different geometric angles of attack at $U_\infty = 45$ m/s.

Effect of angle of attack on noise

This section explains the effect of the geometric angle of attack (α_g) of the various model airfoils on noise attenuation. Experiments are carried out by varying the geometric angles of attack in the range of $-10^\circ \leq \alpha_g \leq 10^\circ$ for the flow velocity of 45 m/s. The corresponding effective angles of attack are estimated to be in the range of $-1.89^\circ \leq \alpha_e \leq 1.89^\circ$.[5] Figure 14 shows the acoustic spectra of the base model airfoil at a different angle of attacks for the flow velocity of 45 m/s. In the case of the base model airfoil, the low frequency noise below 1.3 kHz is sensitive to the angle of attack (Figure 14). The least noise is observed at a $\alpha_g = -10^\circ$, and the noise levels gradually increase up to 5 dB with an increase in the angle of attacks, which is in congruence with the experimental results of Hutcheson and Brooks.[44] The contribution to this noise may be from the suction side of the airfoil, where the boundary layer thickens with an increase in the angle of attack.[5] However, beyond 1.3 kHz, a trend reversal is observed, with not much variation in the spectra except at $\alpha_g = -10^\circ$. Also, similar spectral behaviour is noted for the perforated model airfoils with respect to the angle of attack, as shown in Figure 15. However, the dominance of the low frequency noise with an angle of attack is observed up to 0.6 kHz for all the perforated model airfoils (M1-M4), which is much lower than that observed for the base model airfoil (1.3 kHz). This is because the perforated treatment at the trailing edge changes the flow pattern over the suction side of the airfoil, thereby shifting the reattachment point towards the upstream and thus reducing the interaction of the eddies with the trailing edge.[23] However, beyond 0.6 kHz, a trend reversal is observed with a noise dominance at a lower angle of attack, and a gradual decrease in the noise with an increase of angle of attack. This may be due to the scattering of small-scale structures over the airfoil at lower angles of attacks, which significantly increase the noise level up to 2.2 kHz.

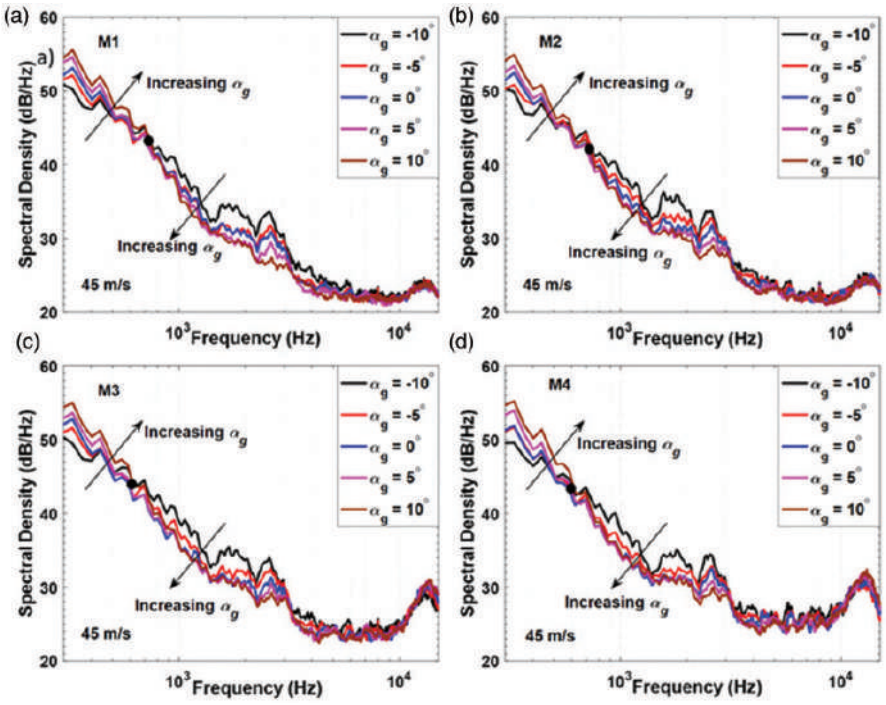

Figure 15. Spectra of perforated model airfoils (a) M1, (b) M2, (c) M3, and (d) M4 at $U_\infty = 45$ m/s at different geometric angles of attack.

Conclusions

In the present study, the NACA6412 airfoil is attached with perforated extension plates at the trailing edge, and its effect on aerodynamic noise is investigated. The pore diameters of these extension plates are varied in the range of 0.689 to 1.665 mm, and the length of the plate extension is 10 mm. Results showed that the perforated model airfoils are significant in reducing the trailing edge noise. The low-frequency noise is observed to reduce with an increase in the pore diameter, and a maximum of 6 –7 dB reduction is noticed for the M4 model airfoil. Subsequently, the perforations also increase the high frequency noise levels, and this noise is observed to be dominant with M3 and M4 model airfoils that have larger pore diameters. A reduction in the overall sound pressure levels by up to 2 dB is noticed with the perforated model airfoils compared to the base model airfoil. The one-third octave spectra of the base model airfoil is observed to scale well with the flow velocity and the displacement boundary layer thickness, and a good collapse is observed in the Strouhal number range of ~ 0.01 and 0.15. Further, ΔSPL spectra showed a good collapse in the lower and higher Strouhal number (based on the pore diameter D) range of $St_D < 0.03$ and $0.1 \leq St_D \leq 0.4$, respectively. An increase in the geometric angle of attack from -10° to $+10^\circ$ increases the noise levels in the lower frequencies, however, increasing the noise levels at higher frequencies. Finally, a set of limited experiments also revealed that the noise emissions depend on the diameter of the pores of the perforated models rather than their open area ratio.

Acknowledgment

The authors would like to sincerely thank the Department of Science and Technology (DST), Govt. of India and Centre for Precision Measurements and Nanomechanical Testing, Department of Mechanical Engineering, National Institute of Technology Calicut, for providing the Alicona optical 3D surface measurement facility purchased under the scheme 'Fund for Improvement of Science and Technology' (FIST – No. SR/FST/ETI-388/2015) during the period of this research work.

Declaration of conflicting interests

The author(s) declared no potential conflicts of interest with respect to the research, authorship, and/or publication of this article.

Funding

The author(s) disclosed receipt of the following financial support for the research, authorship, and/or publication of this article: The authors acknowledge the funding support from the Department of Science and Technology-Science and Engineering Research Board (DST-SERB), grant no. SB/FTP/ETA-0137/2013.

ORCID iD

TJS Jothi https://orcid.org/0000-0002-9674-9045

References

1. Curle N. The influence of solid boundaries upon aerodynamic sound. *Proc R Soc Lond* 1955; A231: 505–551.
2. Ffowcs Williams JE and Hall LH. Aerodynamic sound generation by turbulent flow in the vicinity of a scattering half plane. *J Fluid Mech* 1970; 40: 657–670.
3. Howe MS. A review of the theory of trailing edge noise. *J Sound Vib* 1978; 61: 437–465.
4. Amiet RK. Noise due to turbulent flow past a trailing edge. *J Sound Vib* 1976; 47: 387–393.
5. Brooks TF, Pope DS and Marcolini MA. *Airfoil Self-Noise and prediction*. NASA Reference Publication No. NASA-RP-1218, 1989.
6. Sutliff DL, Tweedt DL, Fite EB, et al. Low-speed fan noise reduction with trailing edge blowing. *Int J Aeroacoustics* 2002; 1: 275–305.
7. Amelda DA and Lee DJ. Effect of external acoustic excitation on NACA0015 discrete tonal noise. *App Acoust* 2018; 141: 374–381.
8. Koike S, Kato H, Kobayashi H, et al. Time-resolved PIV applied to trailing-edge-noise reduction by DBD plasma actuator. In: *27th AIAA aerodynamic measurement technology and ground testing conference*, Chicago, IL, 28 June–01 July 2010, AIAA Paper No. 2010-4352.
9. Arce León C, Ragni D, Pröbsting S, et al. Flow topology and acoustic emissions of trailing edge serrations at incidence. *Exp Fluids* 2016; 57: 1–17.
10. Sarradj E and Geyer T. Noise generation by porous airfoils. In: *13th AIAA/CEAS aeroacoustics conference*, Rome, Italy, 20–23 May 2007, AIAA paper 2007-3719.
11. Herr M and Dobrzynski W. Experimental investigations in low-noise trailing-edge design. *Aiaa J* 2005; 43: 1167–1175.
12. Hayden RE. Fundamental aspects of noise reduction from powered-lift devices. SAE Technical Paper No. 730376. 1973.
13. Bohn AJ. Edge noise attenuation by porous-edge extensions. In: *14th aerospace sciences meeting*, Washington DC, USA, 26–28 January1976.
14. Bachmann T, Klän S, Baumgartner W, et al. Morphometric characterisation of wing feathers of the barn owl Tyto Alba pratincola and the pigeon Columba livia. *Front Zool* 2007; 4: 1–15.

15. Chanaud RC, Kong N and Sitterding RB. Experiments on porous blades as a means of reducing fan noise. *J Acoust Soc Am* 1976; 59: 564–575.
16. Fink MR and Bailey DA. Airframe noise reduction studies and clean-airframe noise investigation. NASA Contractor Report No. NASA-CR-159311, 1980.
17. Khorrami MR, Li F and Choudhari M. Novel approach for reducing rotor tip-clearance-induced noise in turbofan engines. *AIAA J* 2002; 40: 1518–1528.
18. Khorrami MR and Choudhari M. Application of passive porous treatment to slat trailing edge noise, NASA Technical Memorandum No. NASA/TM-2003-212416, 2003.
19. Herr M. Design criteria for low-noise trailing-edges. In: *Proceedings of the 13th AIAA/CEAS aeroacoustics conference (28th AIAA Aeroacoustics Conference)*, Rome, Italy, 21–23 May 2007, AIAA paper no. 2007-3470.
20. Herr M and Reichenberger J. In search of airworthy trailing-edge noise reduction means. In: *17th AIAA/CEAS aeroacoustics conference 2011 (32nd AIAA Aeroacoustics Conference)*, Portland, OR, 5–8 June 2011, AIAA paper no. 2011-2780.
21. Geyer T, Sarradj E and Fritzsche C. Porous airfoils: noise reduction and boundary layer effects. *Int J Aeroacoustics* 2010; 9: 787–820.
22. Geyer TF and Sarradj E. Trailing edge noise of partially porous airfoils. In: *20th AIAA/CEAS aeroacoustics conference*, Atlanta, GA, 16–20 June 2014. AIAA paper no. 2014-3039.
23. Bae Y and Moon YJ. Effect of passive porous surface on the trailing-edge noise. *Phys Fluids* 2011; 23: 126101–126101.
24. Jaworski JW and Peake N. Aerodynamic noise from a poroelastic edge with implications for the silent flight of owls. *J Fluid Mech* 2013; 723: 456–479.
25. Herr M, Rossignol K-S, Delfs J, et al. Specification of porous materials for low-noise trailing-edge applications. In: *20th AIAA/CEAS aeroacoustics conference*, Atlanta, GA, 1–19 June 2014, AIAA paper no. 2014-3041.
26. Kisil A and Ayton LJ. Aerodynamic noise from rigid trailing edges with finite porous extensions. *J Fluid Mech* 2018; 836: 117–144.
27. Jiang C, Moreau D, Yauwenas Y, et al. Control of rotor trailing edge noise using porous additively manufactured blades. In: *24th AIAA/CEAS aeroacoustics conference*, Atlanta, GA, USA, 25–29 June 2018, AIAA paper no. 2018-3792.
28. Ali SAS, Azarpeyvand M and Ilário da Silva CR. Trailing-edge flow and noise control using porous treatments. *J Fluid Mech* 2018; 850: 83–119.
29. Carpio AR, Martínez RM, Avallone F, et al. Experimental characterization of the turbulent boundary layer over a porous trailing edge for noise abatement. *J Sound Vib* 2019; 443: 537–558.
30. Zhang M and Chong TP. On the parametric study of wall-normal permeable trailing edges for aerofoil self-noise reduction. In: *AIAA aviation 2020 forum*, Virtual Event, 15–19 June 2020, AIAA Paper No. 2020-2500.
31. Sumesh CK and Jothi TJS. Aerodynamic noise characteristics of a thin airfoil with line distribution of holes adjacent to the trailing edge. *Int J Aeroacoustics* 2019; 18: 496–516.
32. Zhang M and Chong TP. Effects of porous trailing edge on aerodynamic noise characteristics. *Int J Aeroacoustics* 2020; 19: 254–271.
33. Suryadi A, Martens S and Herr M. Trailing-edge noise reduction technologies for applications in wind energy. In. *23rd AIAA/CEAS aeroacoustics conference*, Denver, CO, USA, 5–9 June 2017, AIAA Paper No. 2017-3534.
34. Carpio AR, Avallone F, Ragni D, et al. 3D-Printed perforated trailing edges for broadband noise abatement. In: *25th AIAA/CEAS aeroacoustics conference*, Delft, The Netherlands, 20–23 May, 2019. AIAA paper no. 2019-2458.
35. Guess AW. Calculation of perforated plate liner parameters from specified acoustic resistance and reactance. *J Sound Vib* 1975; 40: 119– 137.

36. Chong TP, Biedermann T, Koster O, et al. On the effect of leading edge serrations on aerofoil noise production. In: *24th AIAA/CEAS aeroacoustics conference*, Atlanta, GA, USA, 25–29 June 2018, AIAA paper no. 2018-3289.
37. Brooks TF and Hodgson TH. Trailing edge noise prediction from measured surface pressures. *J Sound Vib* 1981; 78: 69–117.
38. Drela M. XFOIL: An analysis and design system for Low Reynolds Number airfoils. In: *Conference on Low Reynolds number aerodynamics*, Notre Dame, USA, 5–7 June 1989.
39. Hutcheson FV, Brooks TF, Burley CL, et al. Measurement of the noise resulting from the interaction of turbulence with a lifting surface. In: *17th AIAA/CEAS aeroacoustics conference (32nd AIAA aeroacoustics conference)*, Portland, Oregon, 5-8 June 2011, AIAA Paper no. 2011-2907.
40. Teruna C, Manegar F, Avallone F, et al. Noise reduction mechanisms of an open-cell metal-foam trailing edge. *J Fluid Mech* 2020; 898: A18.
41. Jiang C, Fischer JR, Moreau D, et al. Experimental investigation of novel porous-serrated treatments on airfoil trailing edge noise reduction. In: *25th AIAA/CEAS aeroacoustics conference*, Delft, The Netherlands, 20–23 May 2019, AIAA paper no. 2019-2435.
42. Chong TP, Vathylakis A, Joseph PF, et al. Self-noise produced by an airfoil with non-flat plate trailing-edge serrations. *AIAA J* 2013; 51: 2665–2677.
43. Jing X, Sun X, Wu J, et al. Effect of grazing flow on the acoustic impedance of an orifice. *AIAA J* 2001; 39: 1478–1484.
44. Hutcheson FV and Brooks TF. Effects of angle of attack and velocity on trailing edge noise. *Int J Aeroacoustics* 2006; 5: 31–66.